Test of the Equivalence Principle with Chiral Masses Using a Rotating Torsion Pendulum

Lin Zhu,[1,2] Qi Liu,[1,2,*] Hui-Hui Zhao,[1] Qi-Long Gong,[1] Shan-Qing Yang,[1,2] Pengshun Luo,[1] Cheng-Gang Shao,[1] Qing-Lan Wang,[3] Liang-Cheng Tu,[1,2] and Jun Luo[1,4,†]

[1]*MOE Key Laboratory of Fundamental Physical Quantities Measurements & Hubei Key Laboratory of Gravitation and Quantum Physics, PGMF and School of Physics, Huazhong University of Science and Technology, Wuhan 430074, People's Republic of China*

[2]*TianQin Research Center for Gravitational Physics and School of Physics and Astronomy, Sun Yat-sen University (Zhuhai Campus), Zhuhai 519082, People's Republic of China*

[3]*College of Science, Hubei University of Automotive Technology, Shiyan 442002, People's Republic of China*

[4]*Sun Yat-sen University, Guangzhou 510275, People's Republic of China*

(Received 6 August 2018; revised manuscript received 6 November 2018; published 26 December 2018)

Here we present a new test of the equivalence principle designed to search for the possible violation of gravitational parity using test bodies with different chiralities. The test bodies are a pair of left- and right-handed quartz crystals, whose gravitational acceleration difference is measured by a rotating torsion pendulum. The result shows that the acceleration difference towards Earth $\Delta a_{\text{left-right}} = [-1.7 \pm 4.1(\text{stat}) \pm 4.4(\text{syst})] \times 10^{-15}\ \text{m s}^{-2}$ (1-σ statistical uncertainty), correspondingly the Eötvös parameter $\eta = [-1.2 \pm 2.8(\text{stat}) \pm 3.0(\text{syst})] \times 10^{-13}$. This is the first reported experimental test of the equivalence principle for chiral masses and opens a new way to the search for the possible parity-violating gravitation.

DOI: 10.1103/PhysRevLett.121.261101

The equivalence of gravitational mass and inertial mass, generally called the equivalence principle (EP), is the foundation of a wide class of gravitational theories including Einstein's theory of general relativity (GR) [1]. However, the EP is suggested to be violated for the existence of possible new particles or interactions, such as the composition-dependent forces [2], dilaton in string theory [3], bosons in supersymmetric theories [4], and even the dark matter particles [5,6]. To take into account a particle's intrinsic spin or space-time torsion, both of which GR does not consider, several phenomenological theories [7–10] have also been proposed and provide new roadways for the EP violation.

With these theoretical motivations, the EP has been tested in many different experiments and the precision is pursued to the highest possible [11]. Up to now, the best laboratory (1-σ) tests in terms of the Eötvös parameter are $\eta_{\text{Be-Ti}} = (0.3 \pm 1.8) \times 10^{-13}$ [12] and $\eta_{\text{Be-Al}} = (-0.7 \pm 1.3) \times 10^{-13}$ [13], obtained by using a rotating torsion balance. The *MICROSCOPE* space mission recently reported its first result, $\eta_{\text{Ti-Pt}} = (0.1 \pm 1.3) \times 10^{-14}$ [14], and lunar laser ranging reported $\eta_{\text{Earth-Moon}} = (3.0 \pm 5.0) \times 10^{-14}$ [15]. Moreover, the EP tests are no longer limited with masses of classical different compositions [12–18], but extended to the bodies with different rotations [19], spins [20] or polarizations [21,22], spin orientations [23], and antimatter [24].

This Letter focuses on another new kind of the EP test to explore possible violation of the gravitational parity [25–28], in which the test masses are different in chirality. If the gravitation is odd parity [25,26], two opposite enantiomers will be coupled differently to the left- and right-handed helicity, leading to a violation of the EP. Besides, the choice of chiral masses is partly inspired by the biological homochirality, namely, almost all living cells on Earth are made of a single chiral form [29]. It is still an open fundamental problem of science, and one of its possible sources is the parity-violating gravitation [27].

In order to experimentally search for possible EP violation due to the gravitational parity violation, the torsion pendulum is employed here for its exquisite ability in feeble-force measurements [30]. The pendulum is suspended by a fiber and carries test masses with opposite chirality (called "chiral dipole"). If there is any difference between the accelerations of two opposite enantiomers towards a source (say Earth), a torque will arise. The torque is modulated by continuous rotation of the pendulum at rate ω_s by a rotary stage, and can be expressed as

$$\tau_{\text{EP}}(t) = p_c \Delta a \sin(\phi_a - \omega_s t - \phi_0),$$

where Δa is the chirality-dependent horizontal acceleration difference, ϕ_a is the azimuth of the horizontal gravitational field $\vec{g}_h$, and p_c is the mass moment of the pendulum [31] with an initial azimuth ϕ_0. This torque will periodically twist the pendulum.

The chiral pendulum with a total mass of 64.5 g is shown in Fig. 1. It mainly consists of four test masses and two mirrors, and all of them are glued to five glass square rods. The pendulum has a fourfold azimuthal symmetry and up-down mirror symmetry. Considering the machinability and

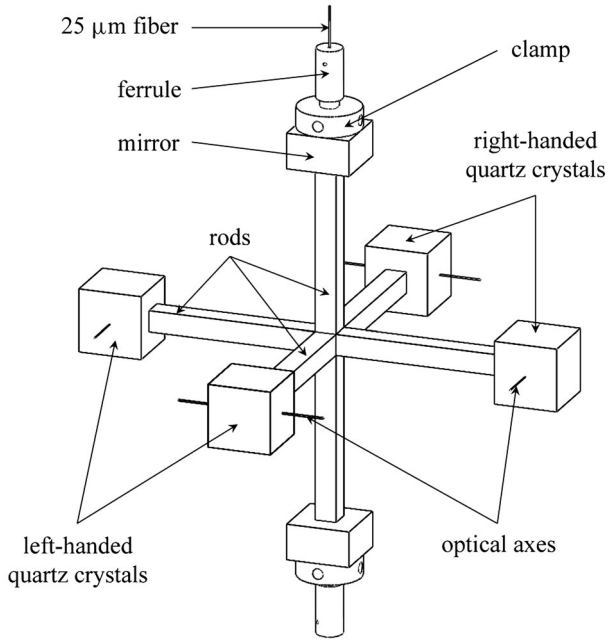

FIG. 1. A schematic drawing of the pendulum. The pendulum carries two left- and two right-handed quartz test masses in a chiral dipole. The orientations of the optical axes are simply aligned horizontal.

magnetic properties, we chose the right- (D) and left (L)-handed quartz crystals [32] as the test masses. The two D- and two L-quartz crystals are all machined into $(1.5\ \mathrm{cm})^3$ cubes. The horizontal distance between any two adjacent cubes is 7.0711(5) cm, each has a mass of 8.936 g, and thus the moment $p_c = 63.2\ \mathrm{g\,cm}$. The optical axes of the crystals are simply aligned in a horizontal plane and in perpendicular to their supporting rods, respectively. After assembling, the pendulum is coated with a thin aluminium layer [33]. The pendulum's moment of inertia about the fiber $I = 968.8(5)\ \mathrm{g\,cm^2}$.

The whole apparatus is constructed as shown in Fig. 2 on the basis of the outstanding design of Eöt-Wash group [12]. The pendulum is suspended by a 25 μm thick, 0.89 m long tungsten fiber and its free torsional oscillation period $T_0 = 784$ s. The top end of the fiber is attached to a magnetic damper to suppress the unwanted swing oscillation. The pendulum is enclosed in an aluminum chamber with a base vacuum $\lesssim 5 \times 10^{-5}$ Pa maintained by an ion pump. The angular position of the pendulum is recorded by an autocollimator [34]. The optical beam of the autocollimator is reflected from one surface of the upper mirror of the pendulum. The chamber is mounted below an air bearing rotary stage [35]. To cancel the gravitational gradient, compensating masses are installed carefully around the pendulum. To decrease the magnetic field and its gradients, the pendulum is surrounded by four layers of magnetic shield fixed with respect to the chamber and one layer of nonrotating magnetic shield [31]. To reduce the disturbance of temperature fluctuation

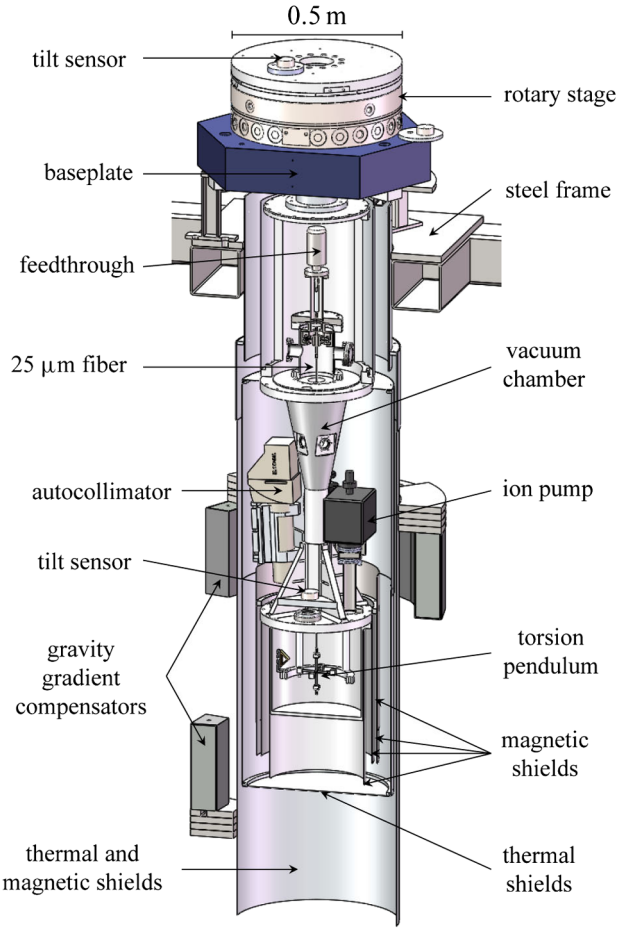

FIG. 2. Cross section of the apparatus. The pendulum suspended by a fiber inside a vacuum chamber is continuously rotated by an air bearing rotary stage. Gravity gradient compensators and magnetic and thermal shields are installed around the pendulum to reduce the gravitation gradient, and magnetic and temperature gradient field.

and gradient, the whole chamber is surrounded by one corotating and another stationary aluminum cylinder. The entire apparatus locates in a cave lab with extreme long-term stability of the environmental gravitational, magnetic, and temperature fields [36].

The twist angle of the pendulum and other 31 signals from the sensors are simultaneously recorded every 1 s. Data collection begins only after the free oscillation amplitude of the pendulum drops below 100 μrad. Figure 3 shows a typical power spectral density (PSD) of the torque. The noise floor is very close to the thermal limit dominated by the internal damping with a quality factor $Q \approx 3800$. After the completion of data acquisition, the signal of interest is extracted by the correlation method [37]. First, a digital filter is used to remove the free torsion oscillations and a rotational filter is used to remove the high-order even harmonics, and the quadratic polynomial drift. The filtered data are then cut into segments with a length of two rotation cycles. For each segment, the $\sin(-\omega_s t)$ and $\cos(-\omega_s t)$ component, $\tau_{\sin}$ and $\tau_{\cos}$, are obtained by the least-squares fit.

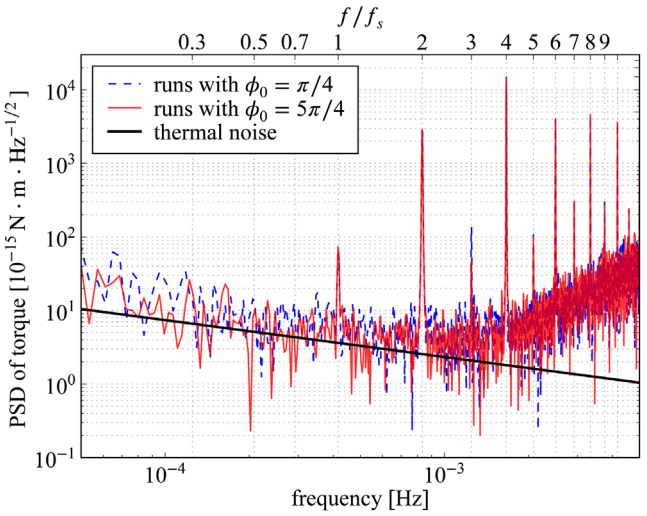

FIG. 3. Typical torque PSDs of the pendulum with different azimuthal angles (blue dashed: $\phi_0 = \pi/4$, red solid: $\phi_0 = 5\pi/4$). The frequency of interest $f_s \approx 0.4167$ mHz, where the noise floor is close to the thermal limit dominated by the internal loss (black heavy). The signal at f_s is mainly due to the systematic effects. The signals at high harmonics ($2f_s, 3f_s, \ldots$) are mainly from the periodic variation of the rotation rate.

Several systematic effects have been investigated carefully. The constancy of the rotation rate is critical in the experiment. The rate is measured by an optical angle encoder (47 200 lines) with two readheads, and then controlled by a servo driver using feedback loops [38]. It is found that the variation of rate originates mainly from the imperfections of the encoder and slightly from the twist of the stage's baseplate. The rate variation can be described by the deviation of the actual rotary angle $\phi(t)$ from the expected $\omega_s t$, $e(t) \equiv \phi(t) - \omega_s t$, which can be expanded into a Fourier series [39]. The rate variation induced spurious signal is from its 1-ω_s harmonic component, $e_1(t) = \nu_a \sin(\omega_s t) + \nu_b \cos(\omega_s t)$. Since it produces a torque $I\ddot{e}_1(t)$ proportional to ω_s^2, the coefficients ν_a, $\nu_b = 85(2), 90(1)$ nrad can be obtained by operating the torsion pendulum at different rotation periods ($T_s = 2\pi/\omega_s = 1200, 1400, \ldots, 2000$ s). To reduce such torque, the rate is turned down to $f_s = 1/T_s \approx 0.4167$ mHz, where the noise floor is still low as shown in Fig. 3.

If the rotary axis of the stage constantly tilts or wobbles at a frequency of $2f_s$ from the local vertical direction defined by the pendulum's gravity, spurious signals will arise. The tilt and wobble are monitored by two corotating biaxial tilt sensors, one near the pendulum and one on the top of the stage. To calibrate the torque response to the tilt (tilt response matrix), we deliberately enlarge the tilt to about 50 μrad by tuning the length of the stage's legs. The calibration shows that a 1-μrad tilt introduces a torque of $1.506(5) \times 10^{-16}$ N m in amplitude. During normal runs, the tilt is adjusted to $\sim$1 μrad which is limited by the fine-tuning of the screws. In addition, the tilt is found to change (≤ 1 μrad) with the fluctuation of ambient temperature, so that we have to correct the instantaneous tilt. To calibrate the response to the 2-f_s wobble (wobble response matrix), three piezo actuators are installed symmetrically under the baseplate of stage. Their heights are periodically changed at $2f_s$ simultaneously. The results show that the magnitude of the wobble response is $\approx 1.4 \times 10^{-16}$ N m/μrad. The wobble in normal runs is about 30 nrad in amplitude and the effect is corrected.

The torque acting on the pendulum induced by the ambient magnetic field will produce a false signal. The nonmagnetic pendulum is found to have extremely rare magnetic impurity described by magnetic dipole μ and quadrupole moments m_{xz}, m_{yz} [31]. The dipole $\mu \approx 4.1$ nA m^2 is measured by the response of the pendulum to the change of the magnetic field produced by a pair of coils. Similar measurements give $m_{xz}, m_{yz} \approx 13$ pAm^3. The magnetic shields reduce the field and field gradient from 22 μT, $\sim$100 nT/cm to 1.9(1) nT, $\sim$0.1 nT/cm, respectively. The correction from the residual field is made and the gradient effects are negligible.

The local gravitational gradients $Q_{\ell 1}(\ell = 2, 3, \ldots)$ coupling to the pendulum with asymmetry of the mass distribution described by $q_{\ell 1}$ will also induce spurious torques [12]. The moments, $q_{21} \approx 0.135$ g cm^2, $q_{31} \approx 0.99$ g cm^3, and $q_{41} \approx 65$ g cm^4, are measured by the responses of the pendulum to the changes of each exaggerated gradient by placing different masses, respectively. The field gradient is measured by another specially designed pendulum more sensitive to the gradient. The gradient Q_{21} is decreased to 0.013(1) g cm^{-3} after being compensated by the masses consisting of about 456 kg of lead blocks and 138 kg of steel plates [40], where the uncertainty is estimated by the monthly variation in continual measurements. Other measurements give $Q_{31} \approx 2.5 \times 10^{-4}$ g cm^{-4} and $Q_{41} \approx 4.6 \times 10^{-5}$ g cm^{-5}. The contribution of residual Q_{21}, Q_{31}, and Q_{41} are all corrected, and the higher order effects are insignificant.

The effect of temperature gradient is also estimated. The torque signal of interest is measured as a function of the temperature gradient which is changed by two large temperature-controlled copper plates in place of the outmost stationary thermal and magnetic shields. The result shows the sensitivity is $2.6(4) \times 10^{-17}$ N m/(K m^{-1}). The gradient in normal runs is ≤ 0.02 K/m, which is limited by the accuracy of the temperature sensor. Conservatively, we take the maximum value of estimation as the uncertainties.

We accumulated the EP data in two sets, one with $\phi_0 = \pi/4$ and the other with $\phi_0 = 5\pi/4$. The 180° change of the orientation of the chiral dipole with respect to the autocollimator is used to cancel the possible unknown effects associated with the torsion fiber or the magnetic damper. For each set, the above systematic effects are fully evaluated (Table I). The data collected during the rapid change of ambient temperature or earthquakes are

TABLE I. Error budgets of the experiments, unit: 10^{-17} N m. Uncertainties are 1-σ.

Error sources	$\phi_0 = \pi/4$		$\phi_0 = 5\pi/4$	
	$\tau_{\sin}$	$\tau_{\cos}$	$\tau_{\sin}$	$\tau_{\cos}$
Measurement and statistical uncertainty	5.32 ± 0.42	-8.33 ± 0.39	22.34 ± 0.32	18.76 ± 0.34
Tilt	-5.21 ± 0.06	-16.57 ± 0.06	24.36 ± 0.09	15.32 ± 0.09
Wobble	-0.50 ± 0.03	0.29 ± 0.03	-0.64 ± 0.03	-0.09 ± 0.03
Rotation rate variation	5.63 ± 0.11	5.98 ± 0.12	5.63 ± 0.11	5.98 ± 0.12
Magnetic field	-0.84 ± 0.04	0.12 ± 0.04	0.85 ± 0.05	-0.21 ± 0.05
$q_{21}Q_{21}$ coupling	6.55 ± 0.13	-1.31 ± 0.13	-4.21 ± 0.13	3.86 ± 0.13
$q_{31}Q_{31}$ coupling	-0.57 ± 0.05	-0.16 ± 0.05	0.25 ± 0.02	0.04 ± 0.02
$q_{41}Q_{41}$ coupling	1.86 ± 0.17	4.78 ± 0.17	-2.51 ± 0.19	-5.20 ± 0.19
Temperature gradient	0.00 ± 0.06	0.00 ± 0.06	0.00 ± 0.06	0.00 ± 0.06
Corrected [a]	$-1.60 \pm 0.42 \pm 0.26$	$-1.46 \pm 0.39 \pm 0.27$	$-1.39 \pm 0.32 \pm 0.28$	$-0.94 \pm 0.34 \pm 0.28$

[a]The first uncertainty is the statistical shown in Fig. 4, and the second is systematic.

excluded, and finally two data sets with a length of about 31 and 50 days are used for $\phi_0 = \pi/4$ and $\phi_0 = 5\pi/4$, respectively.

After the above systematic effects are corrected, a small signal with a magnitude of $\sim 2 \times 10^{-17}$ N m is observed in both sets, as Fig. 4 shows. It is inferred to be due to the suspension system (torsion fiber, magnetic damper). A reversal of ϕ_0 will cause a phase difference of 180° in the EP-violating torque. Hence, the difference between the corrected torque in the two data sets can give the EP-violating torque,

$$\tau_{\mathrm{EP,sin}} = [-0.10 \pm 0.25(\mathrm{stat}) \pm 0.28(\mathrm{syst})] \times 10^{-17}\ \mathrm{N\,m},$$
$$\tau_{\mathrm{EP,cos}} = [-0.26 \pm 0.26(\mathrm{stat}) \pm 0.28(\mathrm{syst})] \times 10^{-17}\ \mathrm{N\,m},$$

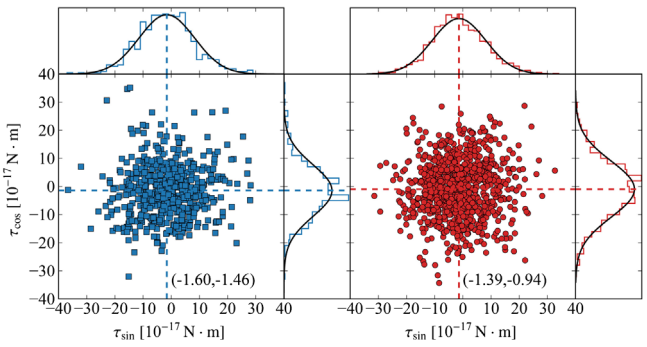

FIG. 4. Scatter plots of the 1-f_s torque of the pendulum with different initial azimuthal angles (left: $\phi_0 = \pi/4$, right: $\phi_0 = 5\pi/4$). The coordinates of every point represent the $\sin(-\omega_s t)$ and $\cos(-\omega_s t)$ component after correction of the systematic effects listed in Table I, and the total numbers of point are 563 and 906, respectively. The insets on the right and top of each main graph give the histograms, and the smooth curves are Gaussian fits. A violation of the EP would cause a difference in the average torque (dashed, shown in brackets) of the two data sets.

where the first uncertainty is statistical, and the second is systematic. The in-phase ($\phi_a - \phi_0 = 3\pi/4$) acceleration difference between D and L quartz towards Earth is

$$\Delta a_{D-L,\mathrm{Earth}} = [-1.7 \pm 4.1(\mathrm{stat}) \pm 4.4(\mathrm{syst})] \times 10^{-15}\ \mathrm{m\,s^{-2}},$$

correspondingly the Eötvös parameter

$$\eta_{D\text{-}L} = \frac{\Delta a_{D-L}}{g_h} = [-1.2 \pm 2.8(\mathrm{stat}) \pm 3.0(\mathrm{syst})] \times 10^{-13}.$$

In conclusion, for the first time, we use the chiral masses as the test bodies to test the EP, and found that the EP is still valid at the level of 10^{-13}. The result can set constraints on the proposed parameters of the odd-parity potential [25,26]. Future improvements are under investigation, including using the fused silica fiber, employing piezo actuators to continuously adjust the tilt, and compensating the gravitational field to be more homogeneous.

The authors wish to acknowledge Li-Di Quan for his work on the speed control, Alan M. Schwartz for drawing our attention to the chirality, and Vadim Milyukov for his helpful discussion. This work was supported by the National Natural Science Foundation of China under Grants No. 91636221, No. 11605065, No. 11475066, No. 11722542, and No. 11325523, and the National Basic Research Program of China under Grant No. 2010CB832804.

*liuq239@sysu.edu.cn
†junluo@sysu.edu.cn

[1] C. M. Will, The confrontation between general relativity and experiment, Living Rev. Relativity **17**, 4 (2014).
[2] E. Fischbach, D. Sudarsky, A. Szafer, C. Talmadge, and S. H. Aronson, Reanalysis of the Eötvös Experiment, Phys. Rev. Lett. **56**, 1427 (1986).
[3] T. Damour, Theoretical aspects of the equivalence principle, Classical Quantum Gravity **29**, 184001 (2012).

[4] P. Fayet, MICROSCOPE limits for new long-range forces and implications for unified theories, Phys. Rev. D **97**, 055039 (2018).

[5] P. W. Graham, D. E. Kaplan, J. Mardon, S. Rajendran, and W. A. Terrano, Dark matter direct detection with accelerometers, Phys. Rev. D **93**, 075029 (2016).

[6] S. M. Carroll, S. Mantry, M. J. Ramsey-Musolf, and C. W. Stubbs, Dark-Matter-Induced Violation of the Weak Equivalence Principle, Phys. Rev. Lett. **103**, 011301 (2009).

[7] Y.-Z. Zhang, J. Luo, and Y.-X. Nie, Gravitational effects of rotating bodies, Mod. Phys. Lett. A **16**, 789 (2001).

[8] I. L. Shapiro, Physical aspects of the space-time torsion, Phys. Rep. **357**, 113 (2002).

[9] W.-T. Ni, Searches for the role of spin and polarization in gravity, Rep. Prog. Phys. **73**, 056901 (2010).

[10] B. Mashhoon, Gravitational couplings of intrinsic spin, Classical Quantum Gravity **17**, 2399 (2000).

[11] A. Sondag and H. Dittus, Electrostatic Positioning System for a free fall test at drop tower Bremen and an overview of tests for the Weak Equivalence Principle in past, present and future, Adv. Space Res. **58**, 644 (2016).

[12] S. Schlamminger, K.-Y. Choi, T. A. Wagner, J. H. Gundlach, and E. G. Adelberger, Test of the Equivalence Principle Using a Rotating Torsion Balance, Phys. Rev. Lett. **100**, 041101 (2008).

[13] T. A. Wagner, S. Schlamminger, J. H. Gundlach, and E. G. Adelberger, Torsion-balance tests of the weak equivalence principle, Classical Quantum Gravity **29**, 184002 (2012).

[14] P. Touboul *et al.*, MICROSCOPE Mission: First Results of a Space Test of the Equivalence Principle, Phys. Rev. Lett. **119**, 231101 (2017).

[15] F. Hofmann and J. Müller, Relativistic tests with lunar laser ranging, Classical Quantum Gravity **35**, 035015 (2018).

[16] S. Fray, C. A. Diez, T. W. Hänsch, and M. Weitz, Atomic Interferometer with Amplitude Gratings of Light and Its Applications to Atom Based Tests of the Equivalence Principle, Phys. Rev. Lett. **93**, 240404 (2004).

[17] A. Bonnin, N. Zahzam, Y. Bidel, and A. Bresson, Simultaneous dual-species matter-wave accelerometer, Phys. Rev. A **88**, 043615 (2013).

[18] L. Zhou, S. Long, B. Tang, X. Chen, F. Gao, W. Peng, W. Duan, J. Zhong, Z. Xiong, J. Wang, Y. Zhang, and M. Zhan, Test of Equivalence Principle at 10-8 Level by a Dual-Species Double-Diffraction Raman Atom Interferometer, Phys. Rev. Lett. **115**, 013004 (2015).

[19] J. Luo, Y. X. Nie, Y. Z. Zhang, and Z. B. Zhou, Null result for violation of the equivalence principle with free-fall rotating gyroscopes, Phys. Rev. D **65**, 042005 (2002); Z. B. Zhou, J. Luo, Q. Yan, Z. G. Wu, Y. Z. Zhang, and Y. X. Nie, New upper limit from terrestrial equivalence principle test for extended rotating bodies, Phys. Rev. D **66**, 022002 (2002).

[20] M. G. Tarallo, T. Mazzoni, N. Poli, D. V. Sutyrin, X. Zhang, and G. M. Tino, Test of Einstein Equivalence Principle for 0-Spin and Half-Integer-Spin Atoms: Search for Spin-Gravity Coupling Effects, Phys. Rev. Lett. **113**, 023005 (2014).

[21] L.-S. Hou and W.-T. Ni, Rotatable-torsion-balance equivalence principle experiment for the spin-polarized $HoFe_3$, Mod. Phys. Lett. A **16**, 763 (2001).

[22] B. R. Heckel, E. G. Adelberger, C. E. Cramer, T. S. Cook, S. Schlamminger, and U. Schmidt, Preferred-frame and CP-violation tests with polarized electrons, Phys. Rev. D **78**, 092006 (2008).

[23] X.-C. Duan, X.-B. Deng, M.-K. Zhou, K. Zhang, W.-J. Xu, F. Xiong, Y.-Y. Xu, C.-G. Shao, J. Luo, and Z.-K. Hu, Test of the Universality of Free Fall with Atoms in Different Spin Orientations, Phys. Rev. Lett. **117**, 023001 (2016).

[24] M. Kimura *et al.*, Testing the Weak Equivalence Principle with an antimatter beam at CERN, J. Phys. Conf. Ser. **631**, 012047 (2015).

[25] P. Bargueño and R. Pérez de Tudela, Constraining long-range parity violation in gravitation using high resolution spectroscopy of chiral molecules, Phys. Rev. D **78**, 102004 (2008).

[26] N. D. H. Dass, Test for C, P , and T Nonconservation in Gravitation, Phys. Rev. Lett. **36**, 393 (1976).

[27] P. Bargueño, Chirality and gravitational parity violation, Chirality **27**, 375 (2015).

[28] S. Alexander and N. Yunes, Chern–Simons modified general relativity, Phys. Rep. **480**, 1 (2009).

[29] N. Jones, Frontier experiments: Tough science, Nature (London) **481**, 14 (2012).

[30] E. G. Adelberger, J. H. Gundlach, B. R. Heckel, S. Hoedl, and S. Schlamminger, Torsion balance experiments: A low-energy frontier of particle physics, Prog. Part. Nucl. Phys. **62**, 102 (2009).

[31] L. Zhu, Q. Liu, H.-H. Zhao, S.-Q. Yang, P. Luo, C.-G. Shao, and J. Luo, Magnetic effect in the test of the weak equivalence principle using a rotating torsion pendulum, Rev. Sci. Instrum. **89**, 044501 (2018).

[32] E. Hecht, *Optics*, 5th ed. (Pearson Education Inc., Boston, MA, 2017).

[33] Q. Li, J.-P. Liu, H.-H. Zhao, S.-Q. Yang, L.-C. Tu, Q. Liu, C.-G. Shao, Z.-K. Hu, V. Milyukov, and J. Luo, G measurements with time-of-swing method at HUST, Phil. Trans. R. Soc. A **372**, 20140141 (2014).

[34] Model ELCOMAT 3000, Möller-Wedel Optical GmbH, Germany, https://www.haag-streit.com/moeller-wedel-optical/products/electronic-autocollimators/elcomat-series/elcomat-3000/.

[35] Model RT500, LAB Motion Systems, Belgium, http://www.labmotionsystems.com/product/rotary-stage-rt500s/.

[36] J. Luo, Q. Liu, L.-C. Tu, C.-G. Shao, L.-X. Liu, S.-Q. Yang, Q. Li, and Y.-T. Zhang, Determination of the Newtonian Gravitational Constant G with Time-of-Swing Method, Phys. Rev. Lett. **102**, 240801 (2009).

[37] D.-H. Wang, J. Luo, and K. Luo, Precise determination of the amplitude of signal with known frequency based on correlated noise model, Rev. Sci. Instrum. **77**, 104501 (2006).

[38] L.-D. Quan, C. Xue, C.-G. Shao, S.-Q. Yang, L.-C. Tu, Y.-J. Wang, and J. Luo, Feedback control of torsion balance in measurement of gravitational constant G with angular acceleration method, Rev. Sci. Instrum. **85**, 014501 (2014).

[39] M. N. Kinnane, L. T. Hudson, A. Henins, and M. H. Mendenhall, A simple method for high-precision calibration of long-range errors in an angle encoder using an electronic nulling autocollimator, Metrologia **52**, 244 (2015).

[40] J.-H. Xu, C.-G. Shao, J. Luo, Q. Liu, L. Zhu, and H.-H. Zhao, Effect of gravity gradient in weak equivalence principle test, Chin. Phys. B **26**, 080401 (2017).